Supporting Information

High-capacity self-sacrificial additive based on electroactive sodiated carbonyl groups for sodium-ion batteries

Zhengna Zhang,[a] Rui Zhang,[a] Ranjusha Rajagopalan,[a] Zheng Tang,[a] Dan Sun,*[a] Haiyan Wang*[a,b] and Yougen Tang*[a]

[a]Hunan Provincial Key Laboratory of Chemical Power Sources, College of Chemistry and Chemical Engineering, Central South University, Changsha, 410083, P. R. China. E-mail: sundan4330@csu.edu.cn, ygtang@csu.edu.cn

[b]School of Chemistry and Chemical Engineering, Henan Normal University, Xinxiang 453007, PR ChinaAddress here.

1. Experimental section

1.1 Synthesis of materials

Preparation of $Na_4C_6O_6$: $Na_2C_6O_6$ was annealed at 400 ℃ under Ar atmosphere for 2 h to obtain the additive sodium salts ($Na_4C_6O_6$) with a navy tinge.[1]

Preparation of Cathode materials: The NVPF/rGO powders were synthesized via the hydrothermal method.[2] All reagents utilized in this study were of analytical grade and employed without further purification. Typically, 364 mg of vanadium pentoxide (V_2O_5) and 648 mg of oxalic acid ($H_2C_2O_4$ $2H_2O$) were dispersed in 30 mL deionized (DI) water stirring at 500 r/min for 20 min, then placed it in an 80 ℃ oil bath and stir vigorously for 1 h. Then, 460 mg of ammonium dihydrogen phosphate ($NH_4H_2PO_4$) and 252 mg of sodium fluoride (NaF) were added into the clear blue solution with vigorous stirring at 70 ℃ for 30 min. Successively, polyvinyl pyrrolidone (K30 Mw ~ 40 000) was added to the above solution until completely dissolved. After that, the 30 mL (2 mg mL^{-1}) graphene oxide (GO, Tanfeng Tech. Inc.) suspension was poured into the above solution under stirring and sonication. The obtained black suspension was

then transferred into a 100 mL Teflon-lined autoclave. The autoclave was sealed and heated in a high-temperature oven at 170 ℃ for 9 h. After naturally cooled down to room temperature, the gel was centrifuged and washed with DI water at 8000 rpm for 3 times. The precipitate was vacuum freeze-dried for 24 h then annealed at 650 ℃ with a heating rate of 5 ℃/min and kept for 2 h in Ar atmosphere. The annealed powder is named as NVPF/rGO sample.

1.2 Preparation of electrode

Preparation of $Na_4C_6O_6$ electrode: Typically, to obtain a uniform binder solution, a certain quantity of polyvinylidene fluoride (PVDF) and N-methyl-2-pyrrolidone (NMP) were mixed and stirred in a magnetic stirrer for 4 hours. Then, tetrasodium of tetrahydroxybenzoquinone ($Na_4C_6O_6$) and Ketjenblack (KB) ($Na_4C_6O_6$, KB and PVDF with a mass ratio of 7:2:1) were added into a binder solution and stirred for 12 h. Uniform slurry was coated on aluminum foil with doctor-blade technique. The electrode was dried at 80 ℃ in a vacuum oven for 12 h and cut into disc pieces with a diameter of 12 mm. The average mass loading of the working electrode was about 1.5 mg cm^{-2}.

Preparation of cathode electrode: The NVPF/rGO electrode was prepared by mixing cathode material $Na_2V_3(PO_4)_3F_2$ (NVPF), KB, and PVDF with the mass ratio of 8:1:1 by a mortar using NMP as a solvent. The obtained slurry was cast on Al sheets with the doctor-blade technique. Analogically, NVPF/rGO-9% was prepared by mixing NVPF, $Na_4C_6O_6$, KB, and PVDF with the mass ratio of 8:1:1:1 by a mortar using NMP as a solvent. And, NVPF/rGO-17% mixing NVPF, $Na_4C_6O_6$, KB, and PVDF with the mass ratio of 8:2:1:1 using NMP as a solvent. Then, the cathode was prepared by drying it in a vacuum oven at a temperature of 80 ℃ for 12 h and the electrodes were obtained by cutting the sheet into a diameter of 12 mm. The average mass loading of the working electrode was about 1.5 mg cm^{-2} for the half-cell, and the mass loading of the cathode electrode was ~3.6 mg cm^{-2} for the full-cell.

Preparation of anode electrode: The slurry was obtained by mixing the commercial hard carbon (HC), super P (SP), and PVDF (with a mass ratio of 8:1:1) in NMP. Then, the slurry was coated onto a copper foil using the doctor-blade technique and dried at

80 ℃ for 12 h in a vacuum oven. Finally, the coated sheet was cut into disks of 12 mm diameter. The average mass loading of the working electrode was ~1.2 mg cm^{-2} for full cell.

1.3 Material characterization: XRD, FT-IR, SEM, and GC-MS

Before characterizing the cycled electrodes, the electrode was immersed in dimethyl carbonate (DMC) for half an hour and dried in a vacuum at room temperature. Scanning electron microscopy (SEM, JSM-7610FPlus) has been used to record the surface morphology of the pre-cycle and post-cycle electrodes. To explore the material structure evolution during charging and discharging, the electrodes were tested using Fourier transform infrared (FT-IR) spectrometer and X-ray diffraction (XRD). The gas components were characterized by Gas Chromatography-Mass Spectrometry (GC-MS).

1.4 Electrochemical measurements:

The electrochemical performances were evaluated by assembling a coin cell. The coin cell was assembled in an argon-filled glove box with water and oxygen content no more than 1ppm. The CR2016-type half cells were assembled with homemade metal sodium tablets as a counter electrode, glass fiber as separator, and 1 M $NaClO_4$ in propylene carbonate (PC) with 5% fluoroethylene carbonate (FEC) as electrolyte. The CR2025-type full cells were assembled in a similar process except HC electrode was used as anode and glass-fiber filter paper as the separator. The mass ratio of HC anode and NVPF-rGO-$Na_4C_6O_6$ cathode is about 1:3. The electrochemical data (cycling performance and rate performance) were performed by Neware CT-3008W battery testing equipment.

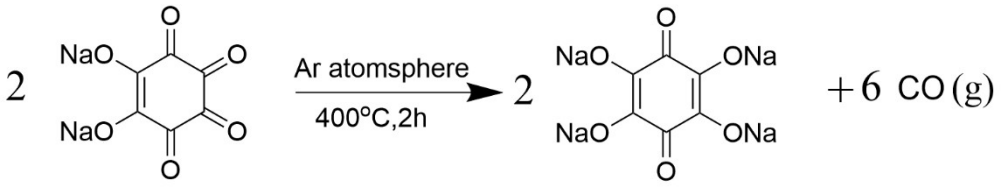

Scheme. S1 commercial $Na_2C_6O_6$ annealing treatment at 400°C for 2h under Ar atmosphere.[1, 3]

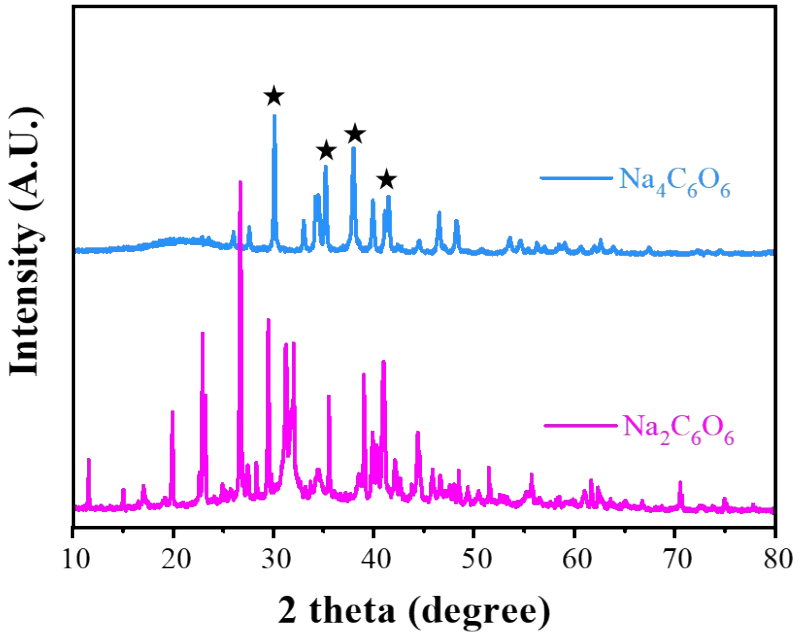

Fig. S1. XRD pattern of $Na_2C_6O_6$ and $Na_4C_6O_6$

The XRD pattern of $Na_2C_6O_6$ is different from $Na_4C_6O_6$. Most of the peaks (27°, 30°, 38° and 40°) of $Na_4C_6O_6$ are similar to $Li_4C_6O_6$, indicating that they have similar crystal structures.[3]

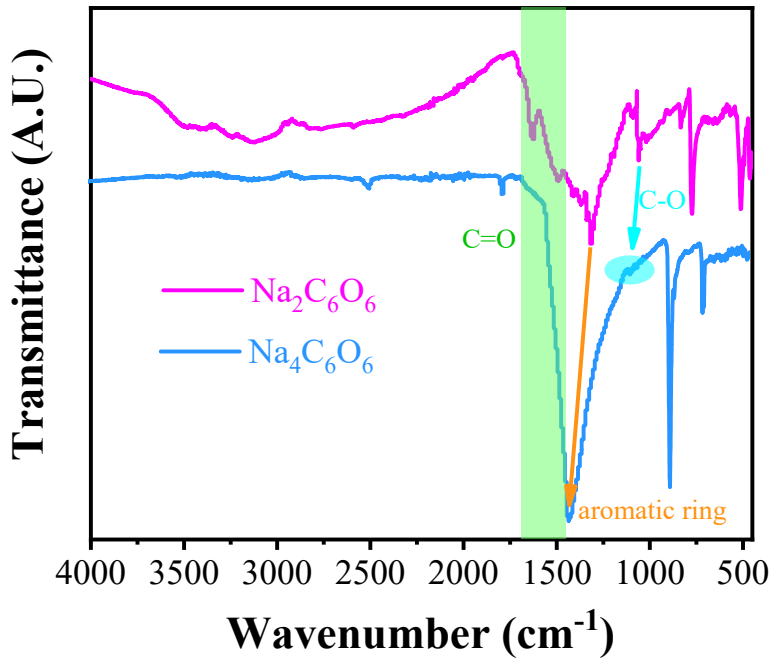

Fig. S2. FT-IR spectra of $Na_2C_6O_6$ precursor and the obtained $Na_4C_6O_6$ samples

The spectra of $Na_2C_6O_6$ and $Na_4C_6O_6$ have significantly different characteristic absorption bands. The two absorption peaks at 1630 and 1490 cm^{-1} in the $Na_2C_6O_6$ spectra can be assigned to the stretching vibration of C=O bond on aromatic ring.[3] In case of $Na_4C_6O_6$, the peak at 1630 cm^{-1} is not very prominent, indicating that a type of C=O retained.

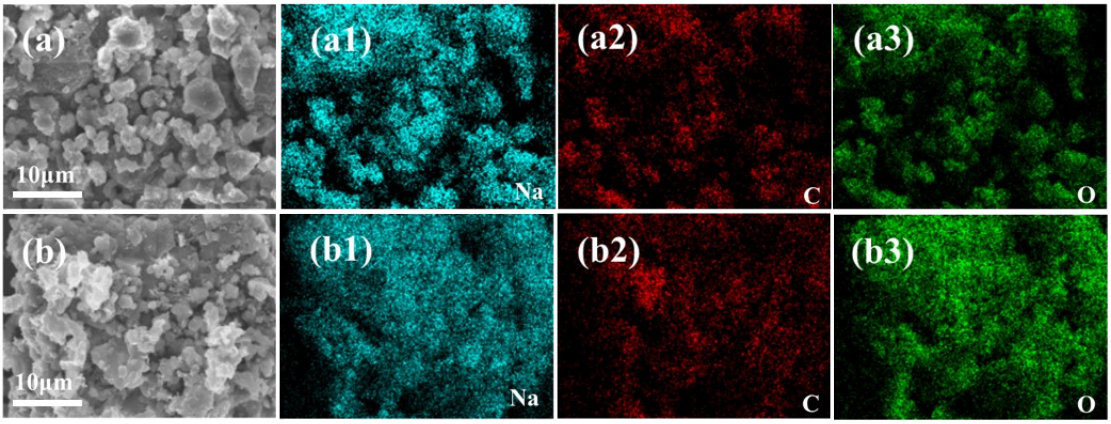

Fig. S3. SEM images and energy dispersive X-ray spectroscopy (EDX) of $Na_2C_6O_6$ and $Na_4C_6O_6$. a) SEM images of $Na_2C_6O_6$ power and corresponding elemental mapping images of Na, C and O; b) SEM images of $Na_4C_6O_6$ power and corresponding elemental mapping images of Na, C and O.

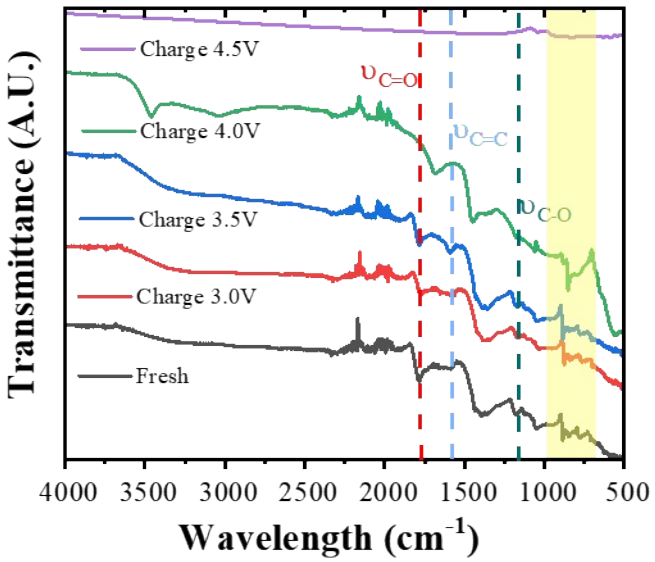

Fig. S4. FT-IR of $Na_4C_6O_6$ electrode charged to different voltages.

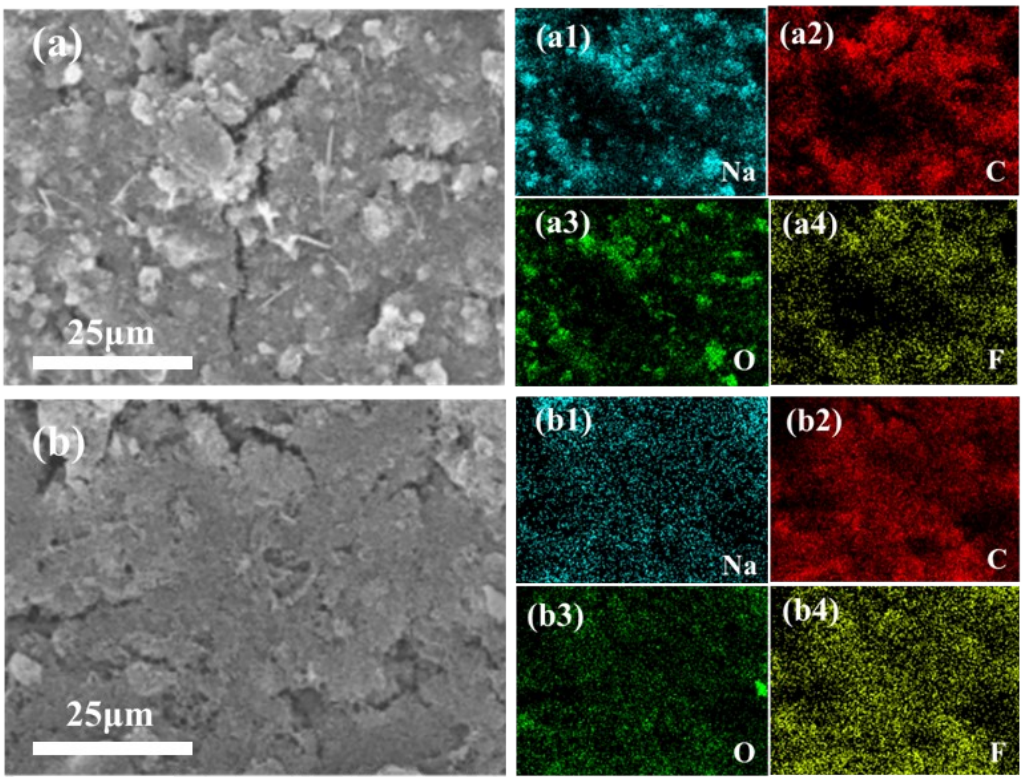

Fig. S5. SEM images of $Na_4C_6O_6$ electrode (a) before and (b) after cycling. EDX mapping images (Na, O, C, F) of (a1-a4) before and (b1-b4) after cycling.

Table. S1 The elemental contents of Na, O, C and F in $Na_4C_6O_6$ electrode before and after cycling.

Element percent (wt.%)/ Sample	**$Na_4C_6O_6$ before**	**$Na_4C_6O_6$ after cycling**
Na	12.2	1.7
C	61.6	72.4
O	19.3	13.0
F	6.8	12.9

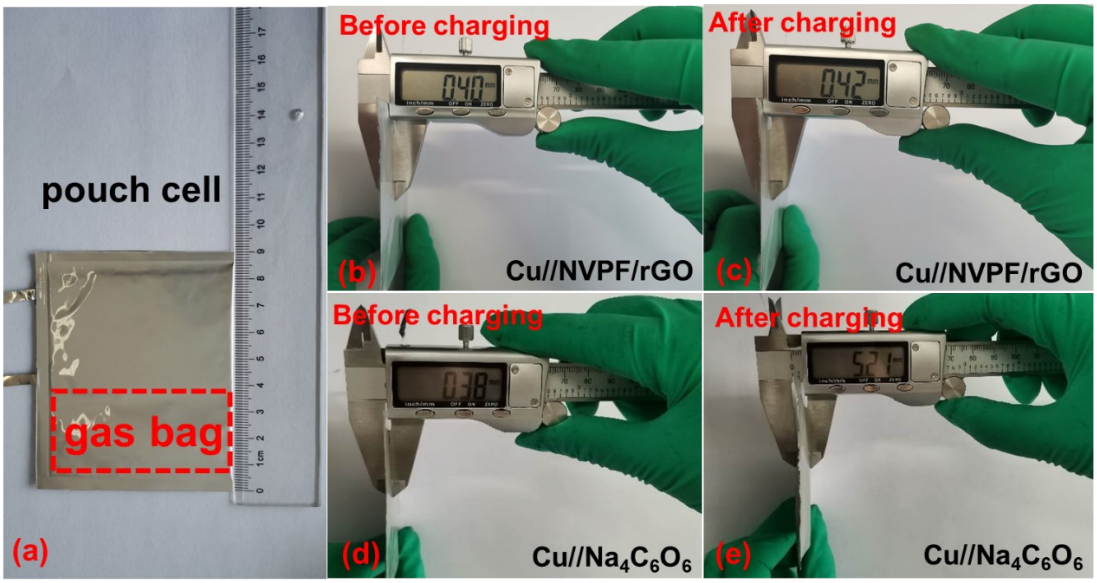

Fig. S6. (a) Digital photos of assembled pouch cell with the copper foil as the reference electrode; the side view of Cu//NVPF/rGO pouch cell (b) before and (c) after charging; the side view of Cu//$Na_4C_6O_6$ pouch cell (d) before and (e) after charging.

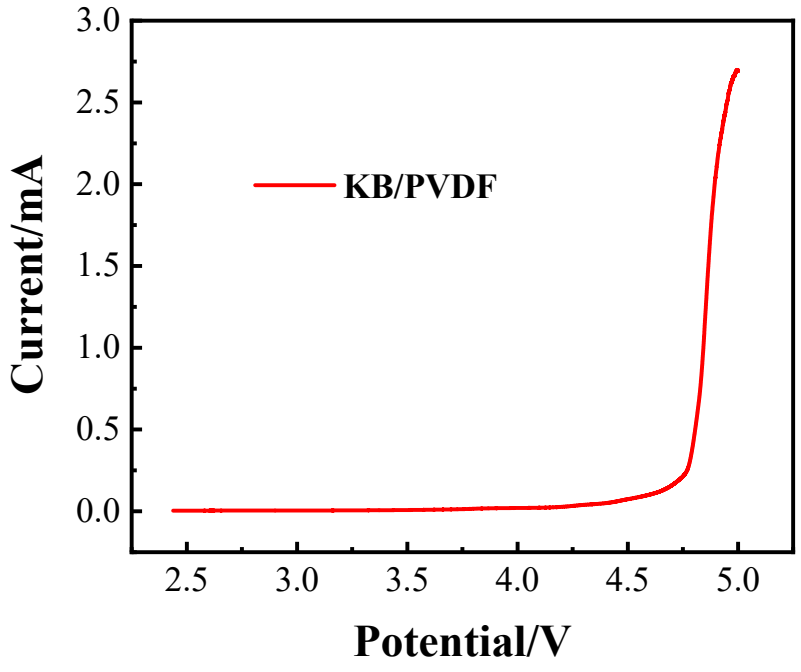

Fig. S7. Linear sweep voltammetry（LSV）curves of Cu//KB/PVDF.

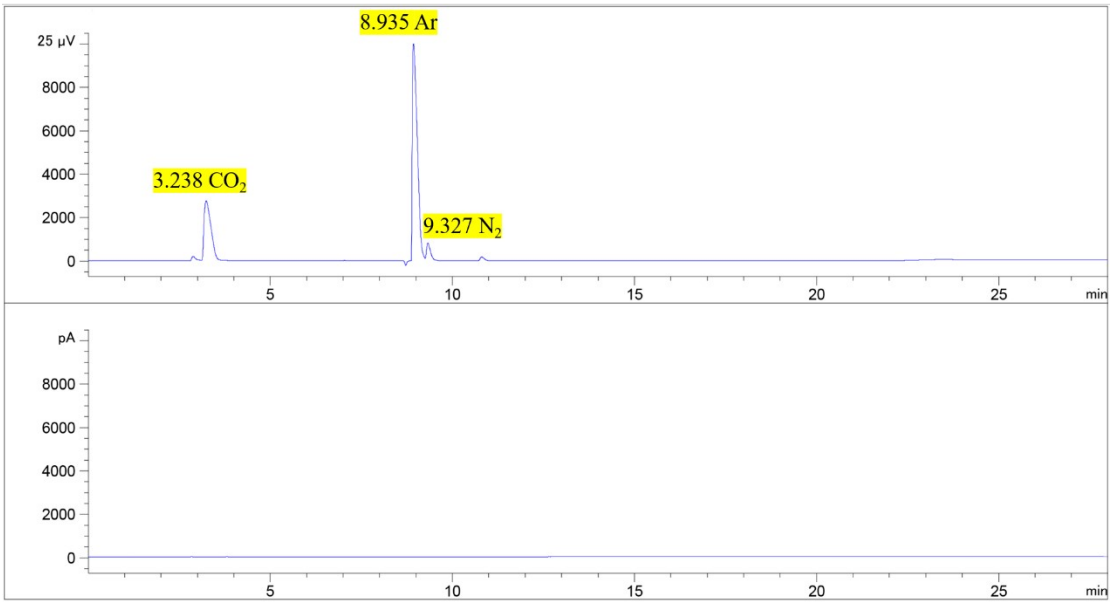

Fig. S8. The GC-MS of CO_2 gases collected in the Cu//$Na_4C_6O_6$ pouch cell after charging 4.5V.

$$Na_4C_6O_6 \rightarrow 3CO_2 + 3C + 4Na^+ + 4e^- \qquad Eq.(S1)$$

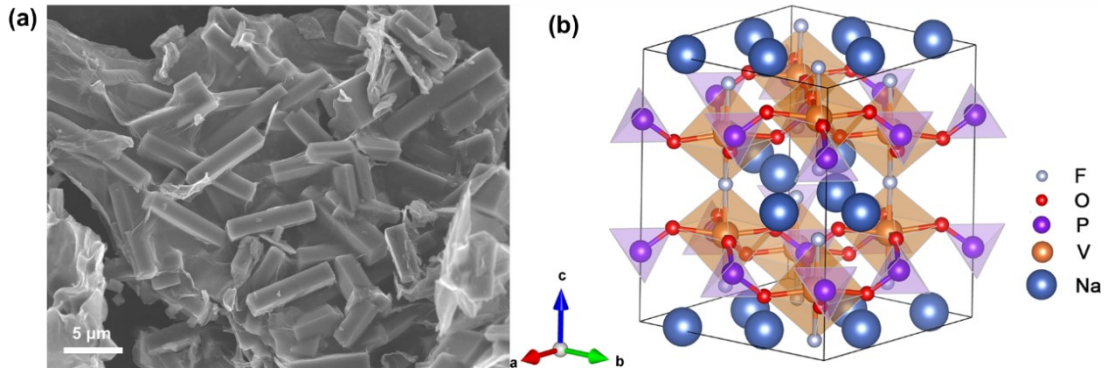

Fig. S9. (a) SEM images of NVPF/rGO power; (b) the crystal structure of NVPF.

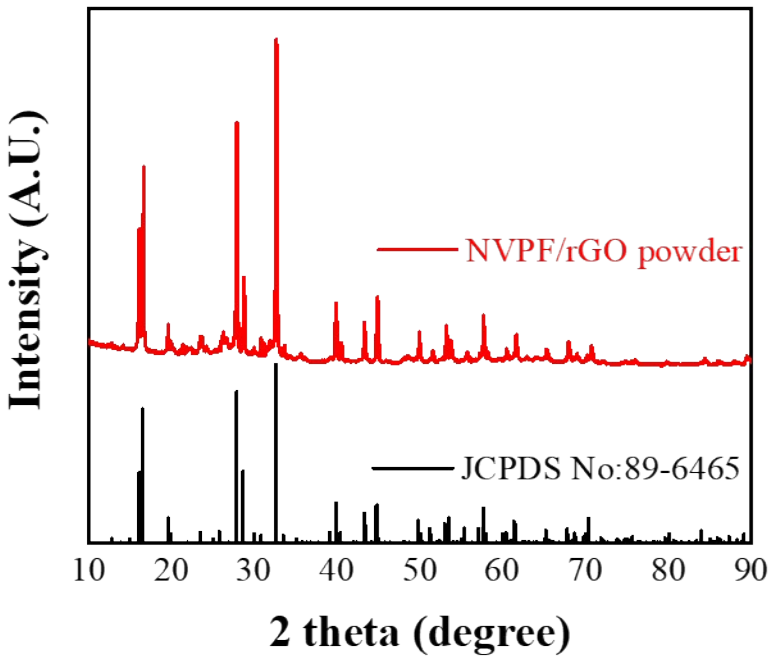

Fig. S10. XRD patterns of NVPF/rGO power.

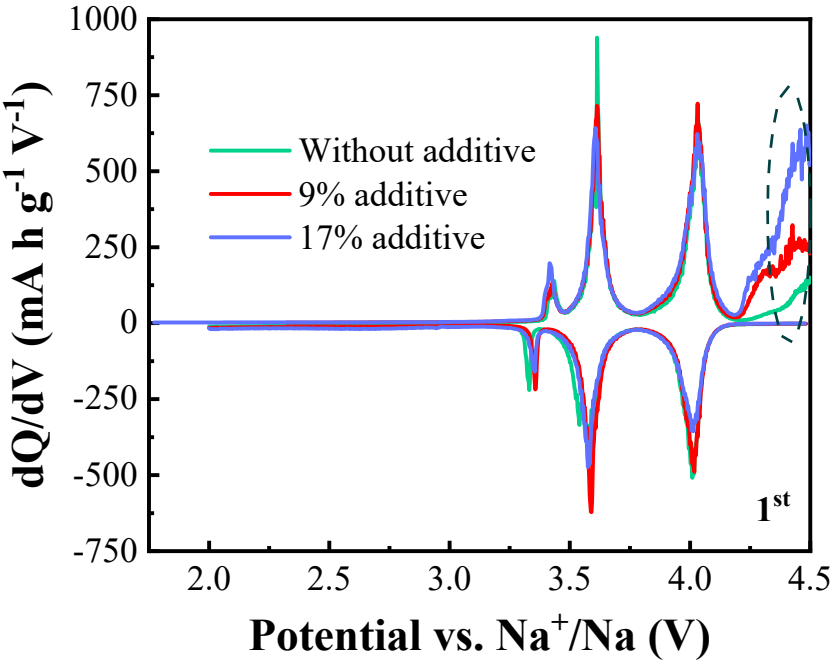

Fig. S11. The first cycle differential capacity curves of NVPF/rGO, NVPF/rGO-9% and NVPF/rGO-17% SIBs at 20 mAg^{-1}.

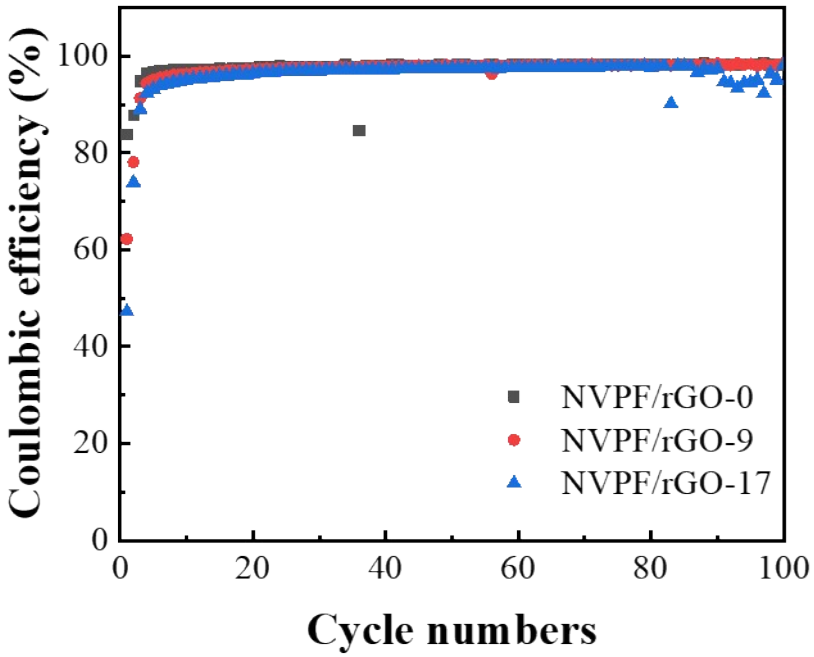

Fig. S12. Comparison of Coulombic efficiencies of half-cells with different amounts of $Na_4C_6O_6$ additives (0 wt%, 9 wt% and 17 wt%) cycled at 50 mA g^{-1}

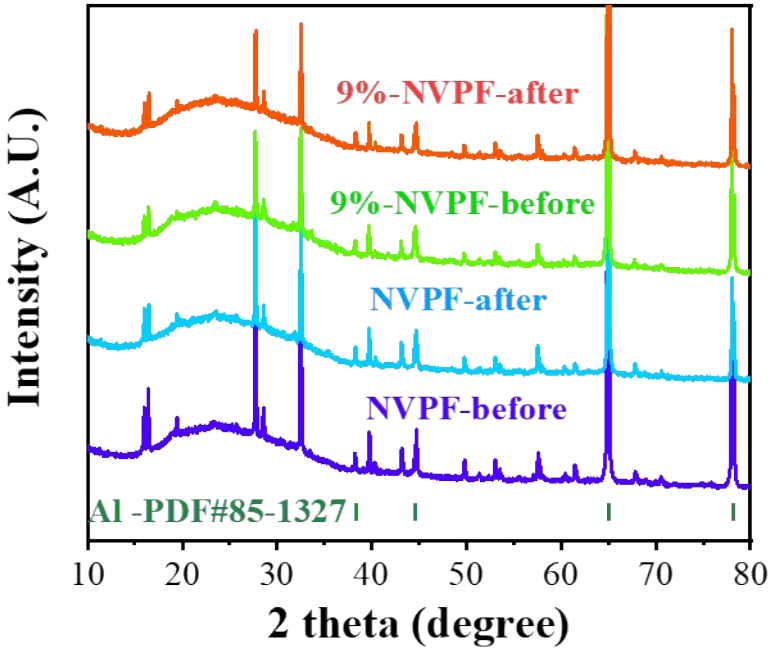

Fig. S13. XRD patterns of NVPF/rGO and NVPF/rGO-9% electrode before and after cycling.

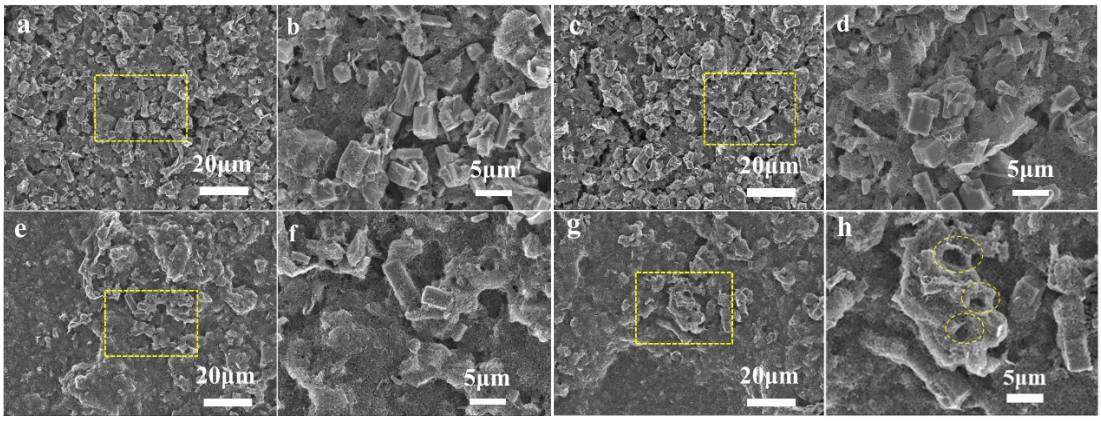

Fig. S14. SEM images of NVPF and NVPF-9% electrode before and after cycling. NVPF electrode (a & b) before and (c & d) after cycling. NVPF-9% electrode (e & f) before and (g & h) after cycling.

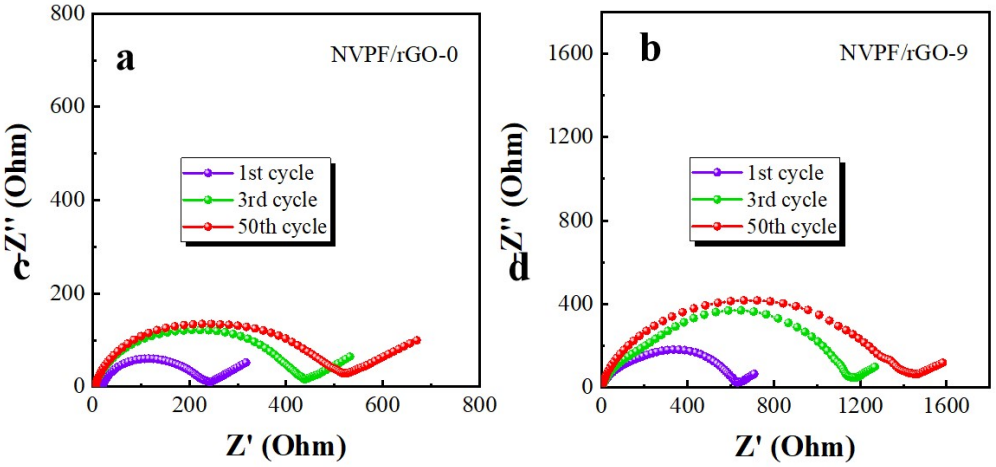

Fig. S15. The EIS plots of NVPF/rGO-0 (a) and NVPF/rGO-9 (b) electrode after different cycles.

The resistances of the cathode before and after adding $Na_4C_6O_6$ were investigated by electrochemical impedance spectroscopy (EIS). As shown in **Fig. S14**, the resistances of NVPF/rGO-9 electrodes are larger than NVPF/rGO electrode, this is due to intrinsically low electronic conductivity of $Na_4C_6O_6$. And with the proceeding of cycles, the resistance of gradually increased, which may have a relationship with multiple factors, such as the formation of interfacial layer, deterioration of electrodes and materials and so on.[4]

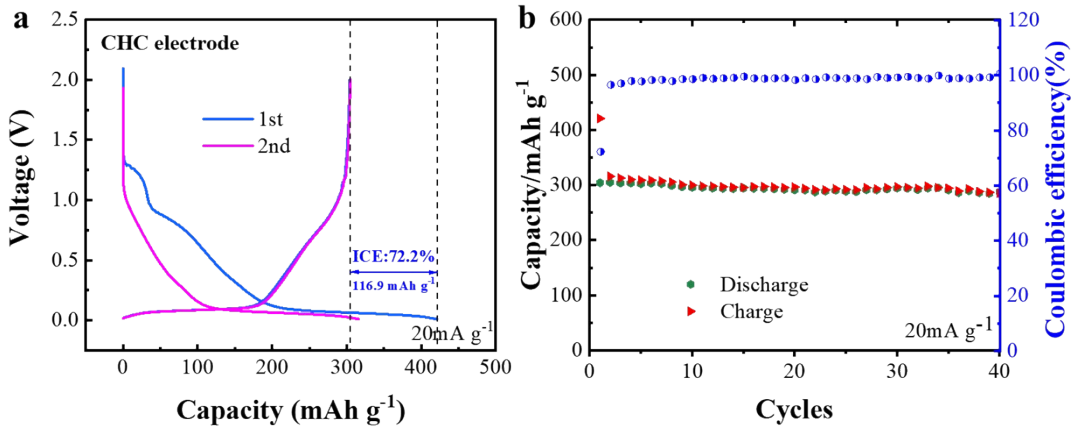

Fig. S16. Electrochemical performance of Na//CHC half-cell at 20 mA g^{-1} (a) galvanostatic charge-discharge profiles; (b) cycling performance and coulombic efficiency curves.

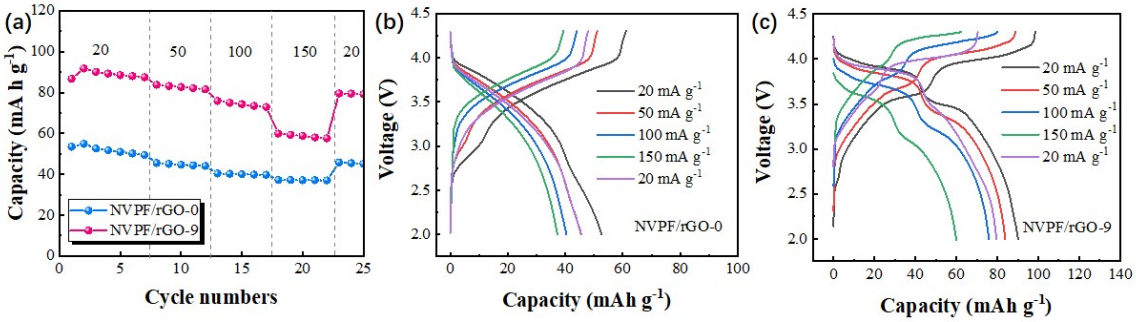

Fig. S17. Rate performance of HC//NVPF/rGO and HC//NVPF/rGO-9% full cells (a). The charge/discharge curves of HC//NVPF/rGO (b) and HC//NVPF/rGO-9% (c) full cells at different current densities. (The capacity is calculated based on the mass of cathode active material)

The rate performance of HC//NVPF/rGO-$Na_4C_6O_6$ full cell was compared in **Fig. S16** at the current densities of 20-150 mA g^{-1}. As seen, the discharge capacities of HC//NVPF/rGO-9% full cell are much higher than those of HC//NVPF/rGO full cell. The charge/discharge curves of HC//NVPF/rGO-9% full cell demonstrate more flat platforms. It should be noted that the performance of full cell has a relationship with a variety of factors, such as cathode, anode, electrolyte, conductive agent and so on. Therefore, to achieve high-performance sodium-ion full cell, more components require optimization.

Table. S2 Comparison of energy densities of reported SIBs with different cathode additives.

ESSs systems	Additive	Amount	Energy density	Reference
HC//P2-NMT SIBs	$Na_2C_2O_4$	10%	215.9 Wh·kg^{-1} at 1C	[5]
HC//NVOPF SIBs	$NaCrO_2$	25.5%	201.5 Wh·kg^{-1} at 0.5C	[6]
HC//P2-NMT SIBs	Na_2O_2	20%	175.0 Wh·kg^{-1} at 0.2C	[7]
HC//NFMO SIBs	NaN_3	20%	161.6 Wh·kg^{-1} at 15 mA·g^{-1}	[8]
HC//NFMO SIBs	$Na_2C_4O_4$	31%	164.9 Wh·kg^{-1} at 15 mA·g^{-1}	[8]
HC//NVPF SIBs	$Na_4C_6O_6$	17%	220.3 Wh·kg^{-1} at 20 mA·g^{-1}	This work
	$Na_4C_6O_6$	9%	210.8 Wh·kg^{-1} at 20 mA·g^{-1}	

Note: This work's energy density was calculated based on the mass of cathode, anode and additive, the others do not extend additive.

Calculation method of full cell energy density:

A. For the HC//NVPF/rGO full cell without additive:

Energy density (Wh kg^{-1}) = Discharge energy of cathode(mWh) *1000 / Mass of cathode, and anode active materials (mg)

B. For the HC//NVPF/rGO-9% and HC//NVPF/rGO-17% full cell with additive:

Energy density (Wh kg^{-1}) = Discharge energy of cathode(mWh) *1000 / Mass of cathode, anode active materials and $Na_4C_6O_6$ (mg)

References

[S1] J. Gu, Y. Gu, S. Yang, *Chem. Commun.* **2017**, 53, 12642.

[S2] Y. Cai, X. Cao, Z. Luo, G. Fang, F. Liu, J. Zhou, A. Pan, S. Liang, *Adv. Sci.* **2018**, 5, 1800680.

[S3] H. Chen, M. Armand, M. Courty, M. Jiang, C. P. Grey, F. Dolhem, J. M. Tarascon, P. Poizot, *J. Am. Chem. Soc.* **2009**, 131, 8984.

[S4] a) S. Liu, W. Lei, Y. Liu, Q. Qiao, W. H. Zhang, *ACS Appl. Mater. Interfaces* **2018**, 10, 37445; b) J. Nie, H. Fu, Z. Li, S. Yao, *J. Alloys Compd.* **2021**, 882, 160693; c) X. Liu, Y. Tan, W. Wang, P. Wei, Z. W. Seh, Y. Sun, *ACS Appl. Mater. Interfaces* **2021**, 13, 27057.

[S5] Y. B. Niu, Y. J. Guo, Y. X. Yin, S. Y. Zhang, T. Wang, P. Wang, S. Xin, Y. G. Guo, *Adv. Mater.* **2020**, 32, e2001419.

[S6] B. Shen, R. Zhan, C. Dai, Y. Li, L. Hu, Y. Niu, J. Jiang, Q. Wang, M. Xu, *J. Colloid Interface Sci.* **2019**, 553, 524.

[S7] Y. J. Guo, Y. B. Niu, Z. Wei, S. Y. Zhang, Q. Meng, H. Li, Y. X. Yin, Y. G. Guo, *ACS Appl. Mater. Interfaces* **2021**, 13, 2772.

[S8] J. Martínez De Ilarduya, L. Otaegui, M. Galcerán, L. Acebo, D. Shanmukaraj, T. Rojo, M. Armand, *Electrochim. Acta* **2019**, 321, 134693.